



**AFRL-RX-WP-JA-2019-0114**

**DISTINGUISHING CRACKS AND NON-METALLIC  
INCLUSIONS USING EDDY CURRENT  
NONDESTRUCTIVE EVALUATION AND (POSTPRINT)**

**John C. Aldrin  
Computational Tools**

**Siamack Mazdiyasni and Matthew R. Cherry  
AFRL/RX**

**Erin K. Oneida and Eric B. Shell  
KBRwyle**

**28 SEPTEMBER 2018  
Interim Report**

**DISTRIBUTION STATEMENT A.  
Approved for public release: distribution is unlimited.**

**© 2019 AUTHOR(S)**

**(STINFO COPY)**

**AIR FORCE RESEARCH LABORATORY  
MATERIALS AND MANUFACTURING DIRECTORATE  
WRIGHT-PATTERSON AIR FORCE BASE, OH 45433-7750  
AIR FORCE MATERIEL COMMAND  
UNITED STATES AIR FORCE**

<b>REPORT DOCUMENTATION PAGE</b>				<i>Form Approved</i> OMB No. 0704-0188	
The public reporting burden for this collection of information is estimated to average 1 hour per response, including the time for reviewing instructions, searching existing data sources, gathering and maintaining the data needed, and completing and reviewing the collection of information. Send comments regarding this burden estimate or any other aspect of this collection of information, including suggestions for reducing this burden, to Department of Defense, Washington Headquarters Services, Directorate for Information Operations and Reports (0704-0188), 1215 Jefferson Davis Highway, Suite 1204, Arlington, VA 22202-4302. Respondents should be aware that notwithstanding any other provision of law, no person shall be subject to any penalty for failing to comply with a collection of information if it does not display a currently valid OMB control number. <b>PLEASE DO NOT RETURN YOUR FORM TO THE ABOVE ADDRESS.</b>					
<b>1. REPORT DATE (DD-MM-YY)</b> 28 September 2018		<b>2. REPORT TYPE</b> Interim		<b>3. DATES COVERED (From - To)</b> 3 March 2014 – 28 August 2018	
<b>4. TITLE AND SUBTITLE</b> Distinguishing Cracks and Non-Metallic Inclusions Using Eddy Current Nondestructive Evaluation (Postprint)				<b>5a. CONTRACT NUMBER</b> IN-HOUSE	
				<b>5b. GRANT NUMBER</b>	
				<b>5c. PROGRAM ELEMENT NUMBER</b>	
<b>6. AUTHOR(S)</b> 1) John C. Aldrin – Computational Tools 2) Siamack Mazdiyasni and Matthew R. Cherry – AFRL/RX (Continued on page 2)				<b>5d. PROJECT NUMBER</b>	
				<b>5e. TASK NUMBER</b>	
				<b>5f. WORK UNIT NUMBER</b> X0UK	
<b>7. PERFORMING ORGANIZATION NAME(S) AND ADDRESS(ES)</b> 1) Computational Tools 4275 Chatham Ave. Gurnee, IL 60031 2) AFRL/RX Wright-Patterson AFB Dayton, OH 45433 (Continued on page 2)				<b>8. PERFORMING ORGANIZATION REPORT NUMBER</b> 1)	
<b>9. SPONSORING/MONITORING AGENCY NAME(S) AND ADDRESS(ES)</b> Air Force Research Laboratory Materials and Manufacturing Directorate Wright-Patterson Air Force Base, OH 45433-7750 Air Force Materiel Command United States Air Force				<b>10. SPONSORING/MONITORING AGENCY ACRONYM(S)</b> AFRL/RXCA	
				<b>11. SPONSORING/MONITORING AGENCY REPORT NUMBER(S)</b> AFRL-RX-WP-JA-2019-0114	
<b>12. DISTRIBUTION/AVAILABILITY STATEMENT</b> DISTRIBUTION STATEMENT A. Approved for public release: distribution is unlimited.					
<b>13. SUPPLEMENTARY NOTES</b> PA Case Number: 88ABW-2018-4871; Clearance Date: 28 Sep 2018. This document contains color. Journal article published in AIP Conference Proceedings, Vol. 2102, 8 May 2019. © 2019 Authors(s). The U.S. Government is joint author of the work and has the right to use, modify, reproduce, release, perform, display, or disclose the work. The final publication is available at <a href="https://doi.org/10.1063/1.5099815">https://doi.org/10.1063/1.5099815</a>					
<b>14. ABSTRACT (Maximum 200 words)</b> Recent work has demonstrated the capability of applying inverse methods to automated eddy current data of surface breaking cracks and notches of various sizes, orientations and aspect ratios. However, not all eddy current indications in turbine engine component inspections originate from cracks, which can result in the unnecessary removal of engine components from service. For powder metallurgy nickel-based superalloys, non-metallic inclusions (NMIs) and non-metallic particles are frequently present. If an EC inspection can reliably classify NMI indications from crack indications, there would be great payoff for the USAF. In this work, simulated results are presented to highlight differences in eddy current signals from cracks and NMIs. Progress is presented on the development of a new model-based inversion scheme highlighting enhancements to the numerical model VIC-3D® and improved indication registration in noisy scans, and the fitting and evaluation of multiple surrogate model classes					
<b>15. SUBJECT TERMS</b> Eddy current; turbine engine; crack; powder metallurgy nickel-based superalloys; non-metallic inclusion (NMI); VIC-3D®,					
<b>16. SECURITY CLASSIFICATION OF:</b>			<b>17. LIMITATION OF ABSTRACT:</b> SAR	<b>18. NUMBER OF PAGES</b> 13	<b>19a. NAME OF RESPONSIBLE PERSON (Monitor)</b> Michael Uchic <b>19b. TELEPHONE NUMBER (Include Area Code)</b> (937) 255-0594
<b>a. REPORT</b> Unclassified	<b>b. ABSTRACT</b> Unclassified	<b>c. THIS PAGE</b> Unclassified			

## REPORT DOCUMENTATION PAGE Cont'd

### 6. AUTHOR(S)

- 3) Erin K. Oneida and Eric B. Shell - KBRwyle
- 4) Harold A. Sabbagh, Elias Sabbagh, and R. Kim Murphy - Victor Technologies
- 5) Alisha L. Hutson - UDRI

### 7. PERFORMING ORGANIZATION NAME(S) AND ADDRESS(ES)

- 3) KBRwyle  
2700 Indian Ripple Rd, Dayton, OH 45440
- 4) Victor Technologies LLC  
2609 S Spicewood Ln., Bloomington, IN 47401
- 5) University of Dayton Research Institute  
300 College Park Ave., Dayton, OH 45469

# Distinguishing Cracks and Non-metallic Inclusions Using Eddy Current Nondestructive Evaluation and Model-Based Inversion

John C. Aldrin<sup>2, a)</sup>, Erin K. Oneida<sup>3</sup>, Eric B. Shell<sup>3</sup>, Harold A. Sabbagh<sup>4</sup>,  
Elias Sabbagh<sup>4</sup>, R. Kim Murphy<sup>4</sup>, Alisha L. Hutson<sup>5</sup>, Siamack Mazdiyasni<sup>1</sup>,  
Matthew R. Cherry<sup>1</sup>,

<sup>1</sup>*Air Force Research Laboratory (AFRL/RXCA), Wright-Patterson AFB, OH 45433, USA*

<sup>2</sup>*Computational Tools, Gurnee, IL 60031, USA*

<sup>3</sup>*KBRwyle, Dayton, OH 45440, USA*

<sup>4</sup>*Victor Technologies LLC, Bloomington, IN 47401, USA*

<sup>5</sup>*UDRI, Dayton, OH 45469, USA*

<sup>a)</sup> [aldrin@computationaltools.com](mailto:aldrin@computationaltools.com)

**Abstract.** Recent work has demonstrated the capability of applying inverse methods to automated eddy current (EC) data of surface breaking cracks and notches of various sizes, orientations and aspect ratios. However, not all eddy current indications in turbine engine component inspections originate from cracks, which can result in the unnecessary removal of engine components from service. For powder metallurgy nickel-based superalloys, non-metallic inclusions (NMIs) and non-metallic particles are frequently present. If an EC inspection can reliably classify NMI indications from crack indications, there would be great payoff for the USAF. In this work, simulated results are presented to highlight differences in eddy current signals from cracks and NMIs. Progress is presented on the development of a new model-based inversion scheme highlighting enhancements to the numerical model VIC-3D®, improved indication registration in noisy scans, and the fitting and evaluation of multiple surrogate model classes. Lastly, inversion results demonstrate the ability to distinguish cracks and NMIs, and the potential to characterize the approximate dimensions and depth of NMIs.

## INTRODUCTION

An important criterion for life management of low cycle fatigue limited turbine engine components is damage tolerance. The use of eddy current (EC) nondestructive evaluation (NDE) techniques to detect damage in aircraft structures and propulsion components is a key part of United States Air Force programs to ensure that the risk of failures meets the desired requirements [1]. Building on early foundational work [2-5], recent progress has demonstrated the capability of characterizing surface breaking cracks and notches of various sizes, orientations and aspect ratios, as well as varying test and probe conditions, using EC NDE with model-based inverse methods [6-12]. However, not all eddy current indications in turbine engine component inspections originate from cracks, which can result in the unnecessary removal of engine components from service. For powder metallurgy nickel-based superalloys, non-metallic inclusions (NMIs) and non-metallic particles (NMPs) are frequently present [13]. If an EC inspection can reliably classify NMI indications from crack indications, especially if the NMI is sub-surface, there would be a great payoff for the USAF. In this paper, simulated results will be presented to highlight differences in eddy current signals from cracks and NMIs with varying depths. The development and application of a model-based inversion scheme for cracks and NMIs will also be presented, to demonstrate the ability to distinguish crack and NMI indications, and the potential to characterize the approximate dimensions and depth of NMIs.

## FIRST-PRINCIPALS ON CLASSIFYING CRACKS AND NMIS

The NDE inspection of cracks and NMIs in this paper was performed using the KBRwyle-developed Eddy Current Inspection Station (ECIS) [7]. All experimental and simulated results were for D20 split-D differential probes, with a size of ~ 20 mils (0.5 mm) operated at 6 MHz. At this frequency, the skin depth for a nickel superalloy is ~ 9.1 mils (0.23 mm). Diagrams of the inspection of parameterized surface crack/notch and NMI models are shown in Fig.

1(a)-1(b). Photos of a notch, a crack and two NMIs [13] are presented in Fig. 1(c)-1(f). Parametric models are expected to adequately represent the key factors influencing the eddy current response of these different discontinuities without requiring an excessive number of variables that might hinder inversion to a ‘global’ solution. NMIs/NMPs are also assumed to contain oxides or air, with low conductivity relative to the substrate. More information on the split-D differential probe model in VIC-3D® can be found in prior work [3,6-12].

Figure 2 shows simulated results for an approximate longitudinal crack, tangential crack and a 5 mil (125  $\mu\text{m}$ ) cuboid NMI, for the horizontal ( $V_x$ ) measurement channel. Note, the simulated horizontal component does provide unique characteristics for all three of flaw shapes / orientations simulated here. These shape characteristics provide promise for the ability to both distinguish and size NMIs from cracks, even for relatively small discontinuities.

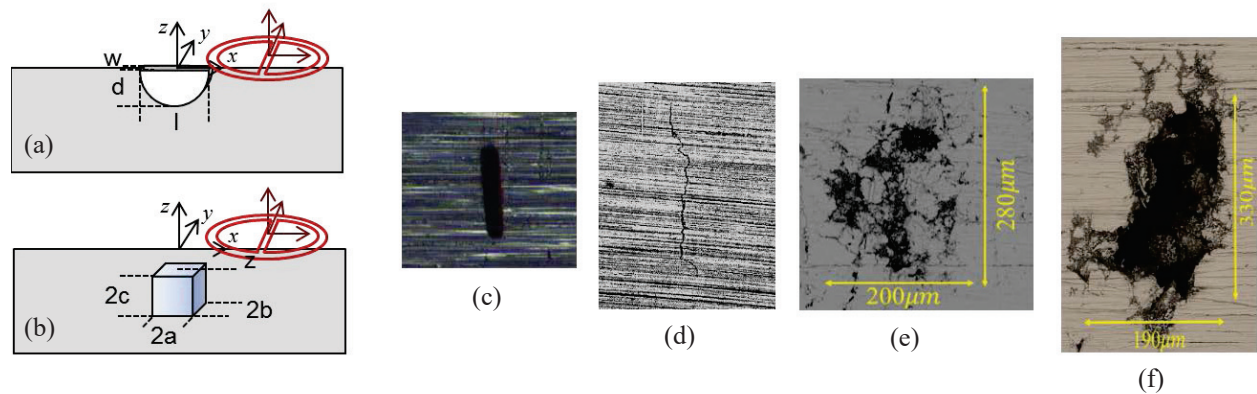


**FIGURE 1.** Diagrams of split-D differential EC probe inspection of parameterized (a) surface breaking crack/notch and (b) approximate NMI models. Example images of (c) notch, (d) surface crack, and surface breaking NMIs [13] with depth of (e) 190  $\mu\text{m}$  and (f) 150  $\mu\text{m}$ .

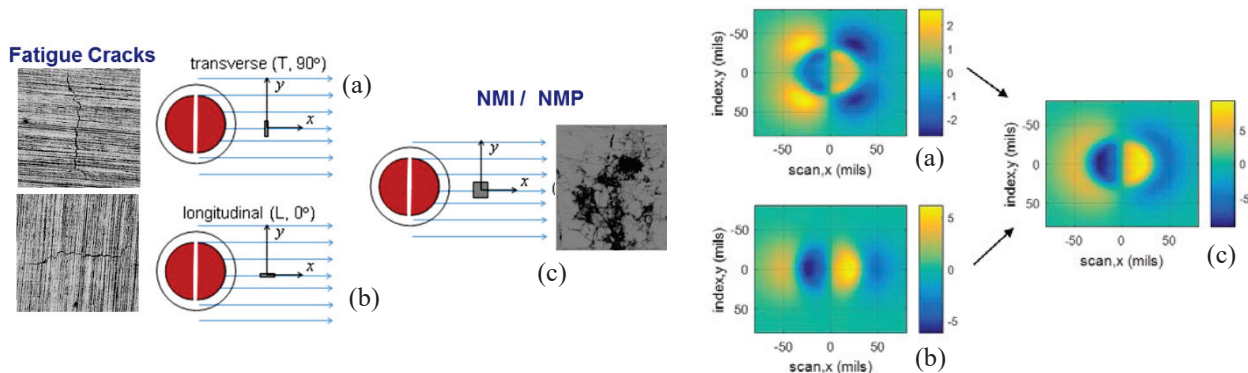


**FIGURE 2.** Diagrams and parametric VIC-3D® simulations of the split-D differential eddy current response for the horizontal component ( $V_x$ ) showing the shape transformation from (a) a transverse and (b) a longitudinal crack/notch (5 x 5 x 1 mil in size, length x depth x width) relative to (c) surface-breaking cubic inclusion / pit (5 x 5 x 5 mil in size).

Figure 3 presents the reactance ( $X$ ) 2D raster scan response for the simulated inclusion model [see Figure 2(a)] with varying depth and size. In these studies, the three size dimensions were fixed to one another, simulating a cuboid. Magnitude of reactance was found to change with both pit size and depth but little to no ‘shape’ changes with respect to inclusion size and depth were observed. Figure 4 presents the impedance plane response ( $R$  vs.  $X$ ) through the peak response ( $y = 0$ ), demonstrating a clear phase change with increasing depth, regardless of size. This ‘phase lag’ characteristic is a classic feature in EM / eddy current signals that enables estimation of the depth of a defect within a substrate [14-21]. Using the maximum impedance plane amplitude and the phase (at this max response), results are presented in Fig. 5 showing the ability to resolve pit depth and size using these two metrics. Note, amplitude is plotted in a dB-scale and at some point, with increasing depth, the response from deep NMIs will be lost in noise.

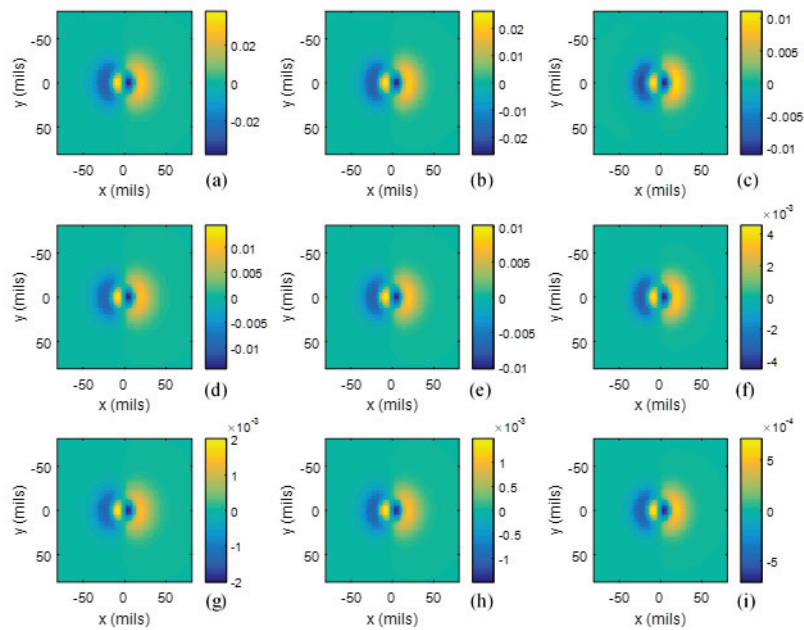


**FIGURE 3.** Reactance ( $X$ , in ohms) 2D raster scan response for a simulated NMIs with varying size ( $2a$ ) and depth ( $z$ ): (a)  $2a=7.5$ ,  $z=1.25$  mils, (b)  $2a=7.5$ ,  $z=2.5$  mils, (c)  $2a=7.5$ ,  $z=5.0$  mils, (d)  $2a=5.0$ ,  $z=1.25$  mils, (e)  $2a=5.0$ ,  $z=2.5$  mils, (f)  $2a=5.0$ ,  $z=5.0$  mils, (g)  $2a=2.5$ ,  $z=1.25$  mils, (h)  $2a=2.5$ ,  $z=2.5$  mils, (i)  $2a=2.5$ ,  $z=5.0$  mils.

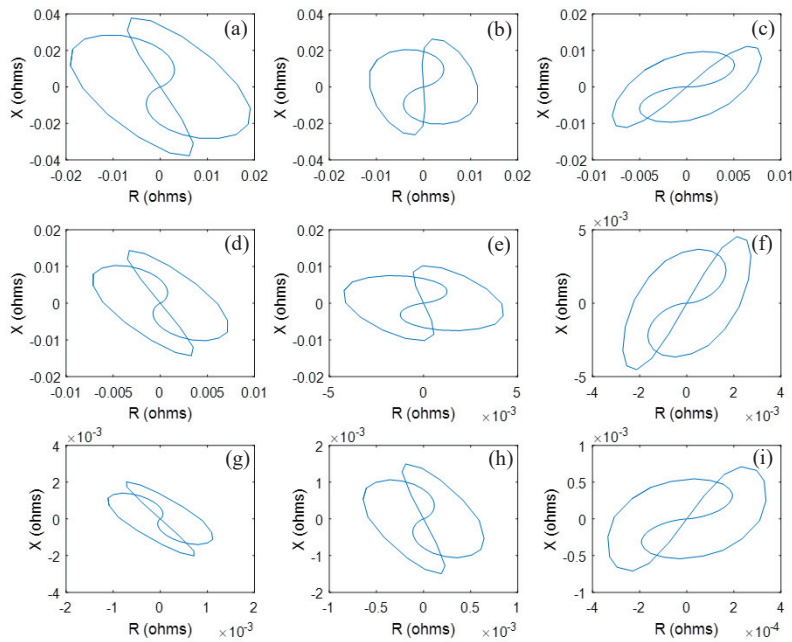


**FIGURE 4.** Impedance plane response (scan in  $x$  direction with  $y = 0$ ) for a simulated inclusion with varying size ( $2a$ ) and depth ( $z$ ): (a)  $2a=7.5$ ,  $z=1.25$  mils, (b)  $2a=7.5$ ,  $z=2.5$  mils, (c)  $2a=7.5$ ,  $z=5.0$  mils, (d)  $2a=5.0$ ,  $z=1.25$  mils, (e)  $2a=5.0$ ,  $z=2.5$  mils, (f)  $2a=5.0$ ,  $z=5.0$  mils, (g)  $2a=2.5$ ,  $z=1.25$  mils, (h)  $2a=2.5$ ,  $z=2.5$  mils, (i)  $2a=2.5$ ,  $z=5.0$  mils.

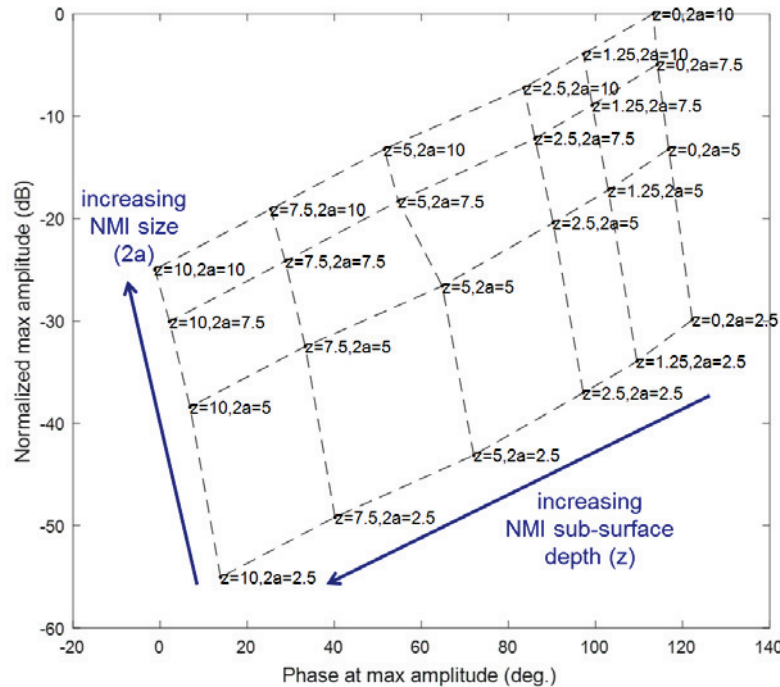


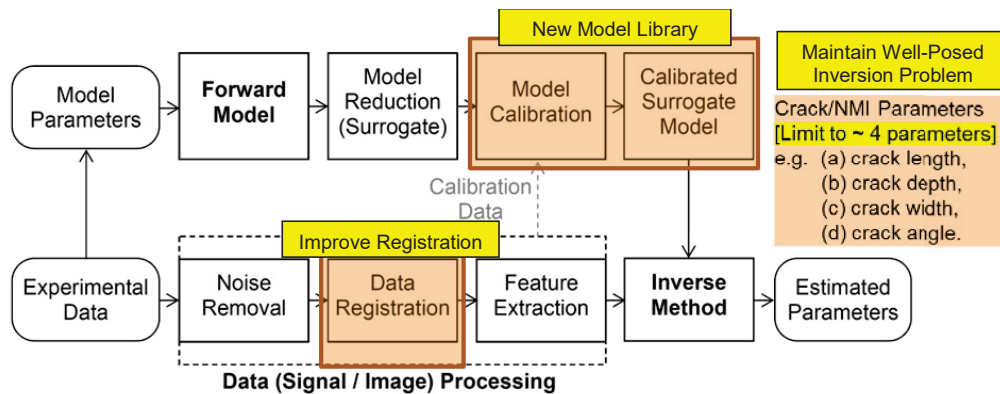
**FIGURE 5.** Normalized maximum impedance plane amplitude and phase (at max. amplitude) for a simulated inclusion with varying depth ( $z$ , in mils) and size ( $2a$ , in mils).

## MODEL-BASED INVERSION PROCESS

The classification problem is to distinguish and size the indication as either a surface breaking crack or an NMI (both surface-breaking and sub-surface) using model-based inversion, leveraging the unique magnitude, phase and shape characteristics of these different classes of discontinuity. The inversion process is presented in Fig. 6. Surrogate models were created using simulated results from VIC-3D® for the D20 split-D differential probe at 6 MHz with a raster scan resolution, at 2 mils x 2.5 mils ( $x, y$ ). Note, refinements to the field extent of the VIC-3D® probe model were made, to address some errors discovered for the tails of the response for small D20 probe. Surrogate models using fast interpolators were implemented to provide the means to improve the speed of the inverse methods. Calibration for all inspections was performed using a single 15 x 8 x 3 mil notch in an IN100 plate. With the calibrated surrogate model, the inversion step can be performed with processed experimental data. A nonlinear least-squares estimator (NLSE) is used to perform the general inversion process in conjunction with an iterative scheme to avoid local minima. Additional details on the base inversion scheme and surrogate model can be found in prior work [6-12].

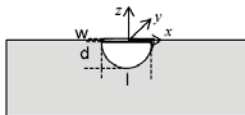
For addressing both cracks and NMIs using a single inversion scheme, several parts of this process were modified (see Fig. 6, highlighted in yellow). First, due to the generally poor signal to noise of small NMI indications considered to date, there was a need to improve registration of the NMI EC feature, essentially improve alignment of the center of the signal in the 2D raster scan for inversion. Second, additional surrogate models covering NMIs, for surface breaking or sub-surface were needed. Lastly, the decision was made to maintain the dimensionality of the inverse problem to a reasonable number of parameters, four, to both minimize the number of required forward model solutions and maintain a reasonable number of parameters to estimate to achieve a more well-posed inversion problem.

Figure 7 presents the new modeling approach, creating three sets of VIC-3D® forward model solutions representing: (a) a semi-elliptical crack/notch, (b) parameterized rectangular cuboid surface inclusion and (c) parameterized rectangular cuboid sub-surface inclusion (where angle is orientation about the  $z$  axis in  $x$ - $y$  plane). This approach addressed some prior difficulty in achieving quality depth estimates of pits that are sub-surface using a single surrogate model for NMIs. By breaking up the surrogate models for surface-breaking NMIs and subsurface NMIs, it enabled greater sensitivity for sizing surface breaking NMIs and also estimating the depth of sub-surface NMIs.



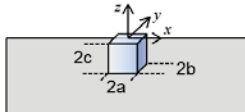
**FIGURE 6.** Diagram of model-based inversion process for 2D eddy current raster scan data from crack/notch and surface/sub-surface inclusions.

(a) Parametric Crack/notch Model



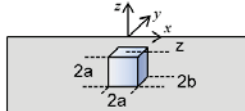
<b>Depth, d (mils)</b>	2.5, 5, 10, 20
<b>Length, l (mils)</b>	5, 10, 15, 20, 25, 30, 40, 60, 80
<b>Width, w (mils)</b>	0.001**, 1, 3, 5
<b>Angle</b>	0°, 30°, 60°, 90°

(b) Parametric Surface Inclusion Model



<b>Pit Size Dim., 2a (mils)</b>	2.5, 5, 7.5, 10
<b>Pit Depth, 2c (mils)</b>	2.5, 5.0, 7.5, 10
<b>Aspect Ratio, a:b (mils)</b>	1:1, 1:2, 2:1
<b>Angle</b>	0°, 30°, 60°, 90°

(c) Parametric Sub-surface Inclusion Model



<b>Size, 2a (mils)</b>	2.5, 5, 7.5, 10
<b>Subsurface Depth, z (mils)</b>	1.25, 2.5, 5.0, 7.5, 10
<b>Aspect Ratio, a:b (mils)</b>	1:1, 1:2, 2:1
<b>Angle</b>	0°, 30°, 60°, 90°

**FIGURE 7.** VIC-3D® forward model solutions for surrogate model: (a) a semi-elliptical crack/notch, (b) a parallelepiped surface non-metallic inclusion and (c) a parallelepiped sub-surface non-metallic inclusion (angle is orientation about z axis in x-y plane).

Figure 8 shows three indications in a nickel-alloy considered to be likely NMIs. For these three likely NMIs indications, they generally exhibited poor signal to noise relative to the scan and material noise signals present in data, as shown in Fig. 9(a). Some surface roughness was observed and polishing of the specimen surface was performed to help remove some of this noise (see Fig. 8). Note, polishing will remove some amount of the top surface, approximately 0.5 to 1 mils, likely reducing the depth of the NMI slightly in the process. Given the generally poor signal to noise from these small indications, there was a need to improve registration of the NMI EC feature, to improve alignment of the center of the signal in the 2D raster scan for inversion. Figure 9 presents a new approach to process experimental data to improve noise removal and better register the center of the data set for comparison to the surrogate model. To help clean up the noise signals that are aligned with the two scan axes, a median filter approach was first applied to fit and remove the underlying regular trends in the background response in the x- and y-directions. Clearer images are achieved as shown in Fig. 9(b). Next, a 2D matched filter was implemented to evaluate the best fit with a typical response from a pit indication. Fig. 9(c) shows the horizontal and vertical components of the eddy current response for a 5 x 5 x 5 mil cuboidal NMI. Example results are presented in Fig. 9(d) for the convolution maps between filtered data and the matched filter. The peak locations in the two convolution maps provide a likely indication of the center of the NMI response. This convolution operation has also been shown to be successful in registering indications from smaller cracks as well.

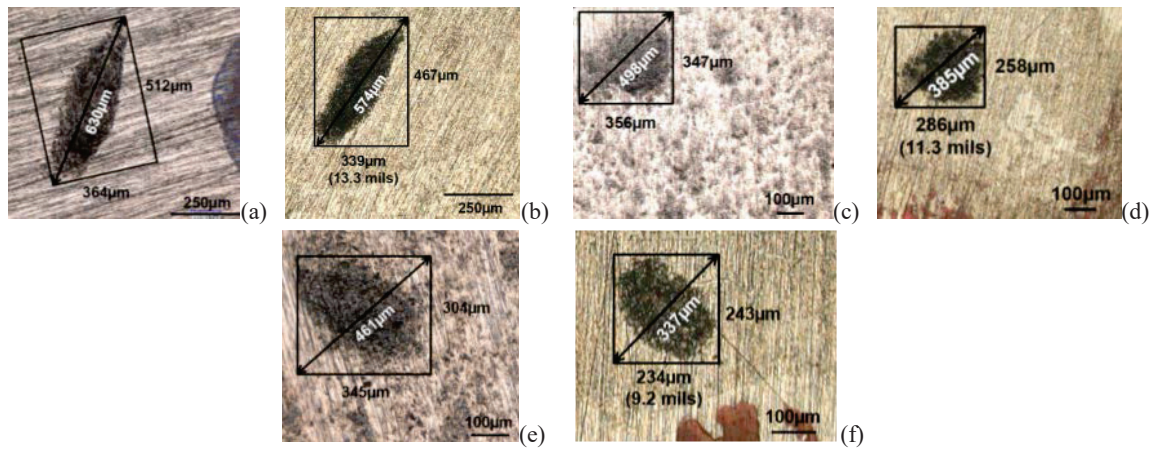


**FIGURE 8.** NMI surface indication #4 (a) before and (b) after polishing, #5 (c) before and (d) after polishing, and #7 (e) before and (f) after polishing.

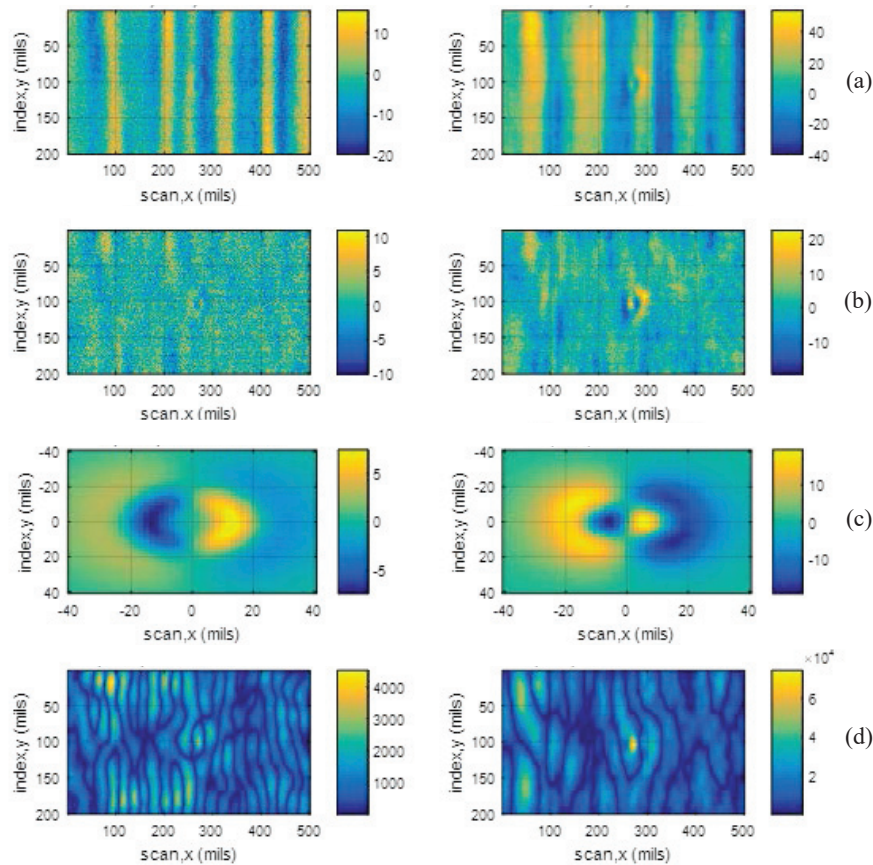


**FIGURE 9.** (a) Experimental eddy current C-scan response for a likely NMI indication embedded in scan noise [LEFT, horizontal component, RIGHT, vertical component], (b) filtered C-scan data, (c) simulated response for a 5 x 5 x 5 mil inclusion used for matched filter, and (d) convolution of filtered C-scan data with matched-filter.

## INVERSION RESULTS

Three test cases for studying the inversion of eddy current data from a semi-elliptical crack/notch, a surface breaking inclusion and a sub-surface inclusion are presented in Tables 1-3 respectively. Case 1 considered experimental ECIS data from a 9.8 x 9.5 mil x 1.2 mil EDM notch. The inversion process was performed using all

three models and quantitative results are shown in Table 1. The crack/notch model was found to produce the best fit based on mean square error (MSE) metric. The two pit models were found to hit constraints on lateral aspect ratio and sub-surface depth, while attempting to best approximate the response of the narrow deep notch that extends from the surface. Error on the inversion of notch length and depth for this case was very good, less than 10% error.

Case 2 considered ECIS data from the likely NMI indication #4 [see Fig. 8(a)], prior to polishing. Again, the inversion process was performed using all three models and quantitative results are shown in Table 2. Both the surface pit and the surface notch models were found to produce the best fits with similar mean square error (MSE) values. A comparison of the best fit model to the experimental results is shown in Fig. 10, for the surface NMI results. Both the crack/notch model and the sub-surface pit model were found to hit constraints on notch width and sub-surface depth respectively; however, the crack/notch model was able to achieve a very similar response to the surface NMI/NMP model due to its small size. Both the notch and surface pit depths estimates were very shallow, estimated to be below 1 mil (25  $\mu\text{m}$ ) in depth. Feedback from the team supports the assertion from the inversion results that these NMIs are very shallow. Future work is planned to grow fatigue cracks from these NMIs following prior work [13], and subsequently perform destructive characterization to provide insight on their true depth.

Due to the lack of a well-controlled test specimen with sub-surface NMIs to date, case 3 considered hybrid data from a simulated sub-surface NMI, with dimensions of 5.75 x 5.75 x 5.75 mils in size, and 4.5 mils in depth, mixed with experimental noise from an unflawed test specimen. These values were chosen because they represent an intermediate point in the surrogate model. Again, the inversion process was performed using all three models and quantitative results are shown in Table 3. The sub-surface pit model was found to correctly produce the best fit based on MSE. A comparison of the best fit sub-surface pit model to the experimental results is shown in Fig. 11. Both the crack/notch model and the surface pit model were found to estimate the response to be quite extreme in aspect ratio and the MSE was about 4 times higher than the sub-surface pit model estimate. Essentially, the surface-breaking flaw models do not exhibit the proper phase / ratio of horizontal to vertical response that is expected from sub-surface discontinuities [compare Fig. 11(c) with respect to Fig. 10(c)], leading to poor inversion fits by MSE. The successful results from cases 1-3 indicate the potential for this inversion scheme to address the proper classification and possible sizing of both cracks and NMIs of varying depth. In particular, the ability to accurately classify large sub-surface NMIs from surface breaking indications is quite positive development.

**TABLE 1.** Inversion results for a 9.8 x 9.5 x 1.2 mil longitudinal orientation EDM notch, using three surrogate model fits.

model	est. depth	est. length	est. width	est. asp.rat.	est. zdepth	est. volume	MSE1	% converge
	mils	mils	mils	()	mils	mils^3		
known	9.5	9.8	1.2	8.2	0.00	112		
crack/notch	9.6	10.4	1.4	7.6	0.00	136	107.0	0.76
surface NMI/NMP	8.7	7.2	3.6	2.0	0.00	223	138.3	0.80
sub-surface NMI/NMP	5.2	10.3	5.2	0.5	1.25	275	176.7	0.55

Hitting constraint in inversion table

**TABLE 2.** Inversion results for a likely NMI indication #4, using three surrogate model fit

model	est. depth	est. length	est. width	est. asp.rat.	est. zdepth	est. volume	MSE1	% converge
	mils	mils	mils	()	mils	mils^3		
known	?	?	?	?	0.00	?		
crack/notch	0.8	9.5	5.0	1.9	0.00	38	5.8	0.39
surface NMI/NMP	0.6	7.1	5.9	0.8	0.00	27	5.8	0.39
sub-surface NMI/NMP	2.5	5.0	2.5	0.5	1.25	32	6.4	0.62

Hitting constraint in inversion table

**TABLE 3.** Inversion results for simulated sub-surface NMI with experimental noise, using three surrogate model fit.

model	est. depth	est. length	est. width	est. asp.rat.	est. zdepth	est. volume	MSE1	% converge
	mils	mils	mils	()	mils	mils^3		
known	5.8	5.8	5.8	1.0	4.50	190		
crack/notch	20.0	1.7	5.0	0.3	0.00	172	11.1	0.86
surface NMI/NMP	10.0	2.6	2.4	1.1	0.00	63	10.0	0.73
sub-surface NMI/NMP	5.7	5.7	5.7	1.0	4.47	187	3.8	0.71

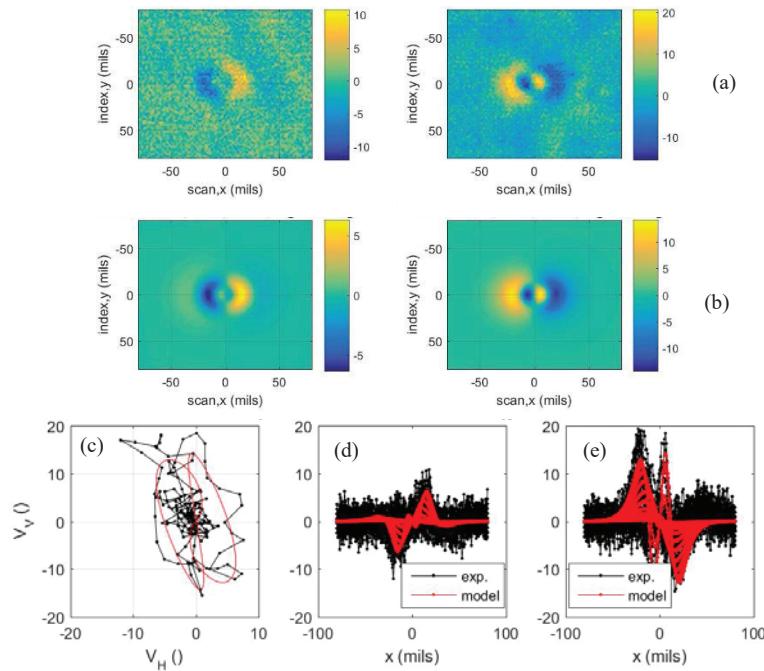


**FIGURE 10.** Model-based inversion for a likely NMI indication #4: (a) ECIS data indication [LEFT, horizontal component, RIGHT, vertical component], (b) VIC-3D® model-based inversion results, (c) impedance plane comparison between model and experiment of peak (x-dir. scan) response, and a comparison for select scan lines of (d) horizontal and (e) vertical components.

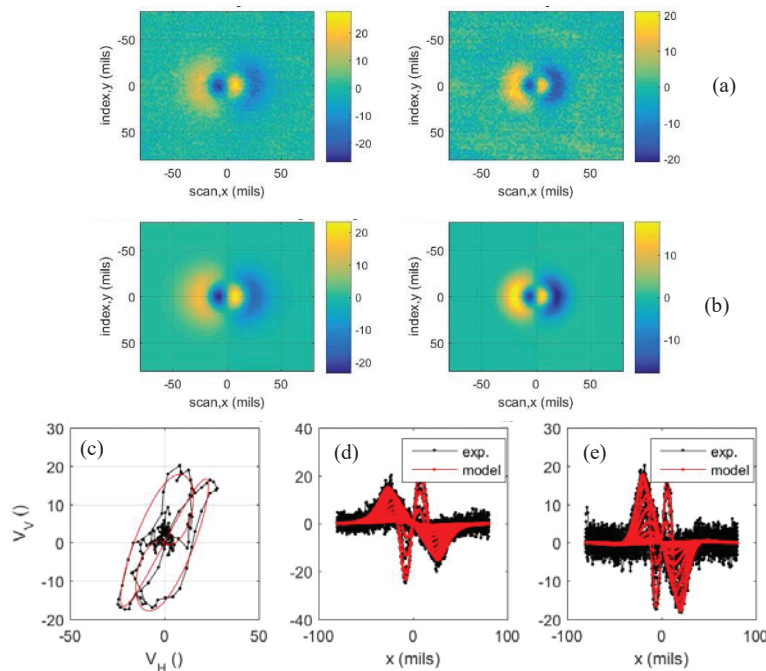


**FIGURE 11.** Model-based inversion of simulated sub-surface NMI: (a) ECIS data indication [LEFT, horizontal component, RIGHT, vertical component], (b) VIC-3D® model-based inversion results, (c) impedance plane comparison between model and experiment of peak (x-dir. scan) response, and a comparison for select scan lines of (d) horizontal and (e) vertical components.

Lastly, additional ECIS data scans from the likely NMI indications #4, #5 and #7 shown in Fig. 8 were acquired. Inversion results are presented in Table 4-6 for the three likely NMIs for varying flaw orientation and different levels

of surfaces polishing. Note, due to poor signal to noise leading to poor registration, one scan failed to achieve quality inversion results. Care is needed in reviewing the output of the inversion process. For these three indications, the pit depths again appear to be very shallow, below 2 mils. There are some trends in the results that indicate a reduction the response due to polish, resulting in some cases of lower estimates for depth and/or volume of the pit. However, the trends with increased polishing are far from perfect. It is expected that precisely estimating the dimensions of such shallow weak indications will be very difficult. However, the inversion process can do a reasonable job of estimating a ‘potential range’ of sizes for NMIs. None of these indications are being called as large cracks or deep large NMIs. Follow-on studies and destructive characterization are planned to ascertain their true depths.

**TABLE 4.** Inversion results for NMI indication #4 from multiple scans and instances of surface polishing.

NMI	model	orientation	est. depth mils	est. length mils	est. width mils	est. asp.rat. ( )	est. zdepth mils	est. volume mils^3	MSE1
4	pre-polish	0	0.8	9.5	5.0	1.9	0.00	38	5.8
4	pre-polish	90	1.2	5.7	4.4	1.3	0.00	30	6.2
4	after polish 1	0	0.4	10.3	8.1	0.8	0.00	33	4.3
4	after polish 1	90	0.4	13.0	6.5	0.5	0.00	35	5.3
4	after polish 2	0	0.3	11.6	8.4	0.7	0.00	31	4.4
4	after polish 2	90	0.3	16.3	8.1	0.5	0.00	34	5.4

**TABLE 5.** Inversion results for NMI indication #5 from multiple scans and instances of surface polishing.

NMI	model	orientation	est. depth mils	est. length mils	est. width mils	est. asp.rat. ( )	est. zdepth mils	est. volume mils^3	MSE1
5	pre-polish	0	1.8	2.6	2.3	0.9	0.00	11	8.2
5	pre-polish	90	1.4	4.3	3.3	1.3	0.00	20	8.9
5	after polish 1	0	1.1	4.4	3.8	1.2	0.00	19	3.9
5	after polish 1	90	0.6	7.4	5.5	1.3	0.00	25	4.5
5	after polish 2	0	0.1	15.7	10.0	1.6	0.00	10	3.6
5	after polish 2	90	0.7	1.9	1.0	0.5	0.00	1	3.7

**TABLE 6.** Inversion results for NMI indication #7 from multiple scans and instances of surface polishing.

NMI	model	orientation	est. depth mils	est. length mils	est. width mils	est. asp.rat. ( )	est. zdepth mils	est. volume mils^3	MSE1
7	pre-polish	0	0.4	19.8	4.6	4.3	0.00	37	5.1
7	pre-polish	90	0.8	6.0	5.5	0.9	0.00	28	5.1
7	after polish 1	0	0.2	12.4	7.4	1.7	0.00	14	3.8
7	after polish 1	90	0.9	2.9	4.6	0.6	0.00	12	4.6

## CONCLUSIONS AND FUTURE WORK

In this work, the problem of distinguishing cracks from non-metallic inclusions was considered. Simulated results were presented that highlight differences in magnitude, phase and shape characteristics of the eddy current signals from cracks and NMIs. Progress was presented on the development of a new model-based inversion scheme highlighting enhancements to the numerical model VIC-3D®, improved indication registration for noisy scans, and the fitting and evaluation of multiple surrogate model classes for classification and characterization. A series of case studies were used to demonstrate the potential for this inversion scheme to address proper classification and possible sizing of both crack and NMIs of varying depth. Future work is planned for growing fatigue cracks from the shallow NMIs presented in this paper, including subsequent destructive characterization to verify their depth. While the sub-surface NMI demonstration using hybrid (model + experimental noise) data was considered a positive first step, verification with physical specimens is needed. Additional test specimens with embedding non-metallic inclusions under a thin top sheet of Waspaloy are under development for future work.

## ACKNOWLEDGMENTS

This work is supported by the U.S. Air Force Research Laboratory (AFRL) through Research Initiatives for Materials State Sensing II (RIMSS II), Inversion of Received Electromagnetic Signals to Characterize Damage in Propulsion Systems, Contract No: FA8650-10-D-5210, Agreement No. 12-S7114-03-C1. The authors would like to

acknowledge technical discussions with Vikas Sinha and Kristin Keller of UES on embedding NMIs in nickel-based super-alloys.

## REFERENCES

1. E. A. Lindgren, J. S. Knopp, J. C. Aldrin, G. J. Steffes, and C. F. Buynak, "Aging aircraft NDE: capabilities, challenges, and opportunities", *Review of Progress in QNDE*, Vol. 26, AIP Conf. Proc., **894**, pp. 1731-1738, (2007).
2. L. D. Sabbagh and H. A. Sabbagh, "Eddy-Current Modeling and Flaw Reconstruction," *J. Nondestructive Evaluation*, **7**, n. 1/2, pp. 95-110, (1988).
3. H. A. Sabbagh, R. K. Murphy, E. H. Sabbagh, J. C. Aldrin, and J. S. Knopp, *Computational Electromagnetics and Model-Based Inversion - A Modern Paradigm for Eddy-Current Nondestructive Evaluation*, Springer, (2013).
4. J. C. Aldrin, H. A. Sabbagh, E. H. Sabbagh, R. K. Murphy, M. Concordia, D. Judd, E. Lindgren, and J. S. Knopp, "Methodology using inverse methods for pit characterization in multilayer structures," *Review of Progress in QNDE*, Vol. 25, AIP, pp. 767-774, AIP Conf. Proc., **820**, (2006).
5. J. C. Aldrin, H. A. Sabbagh, R. K. Murphy, E. H. Sabbagh and J. S. Knopp, "Sensitivity analysis of inverse methods in eddy current pit characterization", *Review of Progress in QNDE*, Vol. 29, AIP Conf. Proc., **1211**, pp. 771-718, (2010).
6. J. C. Aldrin, H. A. Sabbagh, E. H. Sabbagh, R. K. Murphy, M. Keiser, D. S. Forsyth, E. A. Lindgren, "Model-based inverse methods for bolt-holt eddy current (BHEC) inspection", *Review of Progress in QNDE*, Vol. 33, AIP Conf. Proc., **1581**, pp. 631-638, (2014).
7. E. B. Shell, J. C. Aldrin, H. A. Sabbagh, E. H. Sabbagh, R. K. Murphy, S. Mazdiasni and E. A. Lindgren, "Demonstration of model-based inversion of electromagnetic signals for crack characterization," *Review of Progress in QNDE*, Vol. **34**, AIP Conf. Proc., **1650**, pp. 484-493, (2015).
8. E. K. Oneida, E. B. Shell, J. C. Aldrin, H. A. Sabbagh, E. H. Sabbagh, R. K. Murphy, S. Mazdiasni and E. A. Lindgren, "Flaw characterization using inversion of eddy current response and the effect of filters and scan resolution," *42nd Annual Review of Progress in QNDE, Incorporating the 6th European-American Workshop on Reliability of NDE*, AIP Conf. Proc., **1706**, p. 090021, (2016).
9. R. D. Mooers and J. C. Aldrin, "Effects of Angular Variation on Split D Differential Eddy Current Probe Response," *42nd Annual Review of Progress in QNDE, Incorporating the 6th European-American Workshop on Reliability of NDE*, AIP Conf. Proc., **1706**, p. 090022, (2016).
10. J. C. Aldrin, E. B. Shell, E. K. Oneida, H. A. Sabbagh, E. H. Sabbagh, R. K. Murphy, S. Mazdiasni and E. A. Lindgren, "Model-based inverse methods for sizing surface-breaking discontinuities with eddy current probe variability," *42nd Annual Review of Progress in QNDE, Incorporating the 6th European-American Workshop on Reliability of NDE*, AIP Conf. Proc., **1706**, p. 090002, (2016).
11. E. K. Oneida, E. B. Shell, J. C. Aldrin, H. A. Sabbagh, E. H. Sabbagh, R. K. Murphy, S. Mazdiasni and E. A. Lindgren, "Characterizing surface-breaking cracks through eddy current NDE and model-based inversion," *Materials Evaluation*, **75**, n 7, p. 915-929, (2017).
12. J. C. Aldrin, E. K. Oneida, E. B. Shell, H. A. Sabbagh, E. H. Sabbagh, R. K. Murphy, S. Mazdiasni, E. A. Lindgren, and R. Mooers, "Model-based probe state estimation and crack inverse methods addressing eddy current probe variability," *43rd Annual Review of Progress in QNDE*, AIP Conf. Proc., **1806**, p. 110013, (2017).
13. M. R. Cherry, A. Hutson, J. C. Aldrin, and J. Shank, "Eddy current analysis of cracks grown from surface defects and non-metallic particles," *44th Annual Review of Progress in QNDE*, AIP Conf. Proc., **1949**, p. 140007, (2018).
14. D. C. Fraser and S. H. Ward, "Analytic and model studies of a rotatable field electromagnetic prospecting system," *Geophysics*, **32**, n 5, pp. 899-917 (1967).
15. B. Brudar, "How to distinguish surface and subsurface cracks using electromagnetic NDT methods," *NDT International*, **17**, n. 4, pp. 221-223, (1984).
16. G. Van Drunen and V. S. Cecco. "Recognizing limitations in eddy-current testing," *NDT International*, **17**, n.1, pp. 9-17, (1984).
17. D. J. Hagemaijer, *Fundamentals of Eddy Current Testing*, ASNT, Columbia, OH, (1990).
18. H.-J. Krause and M. V. Kreutzbruck, "Recent developments in SQUID NDE," *Physica C: Superconductivity*, **368**, n 1-4, pp. 70-79 (2002).
19. E. N. Shawhan, A. C. Mclean, P. Harry, and R. L. Mather, "Submerged body detection system," *U.S. Patent No. 3,020,470*, U.S. Patent and Trademark Office, Washington, DC, (1962).
20. T. J. Davis and C. B. Perry, "Digitally controlled multifrequency eddy current test apparatus and method," *U.S. Patent No. 4,303,885*, U.S. Patent and Trademark Office, Washington, DC, (1981).
21. N. J. Goldfine, V. A. Zilberstein, D. E. Schlicker, D. C. Grundy, I. C. Shay, R. J. Lyons, and A. P. Washabaugh, "Hidden feature characterization using a database of sensor responses," *U.S. Patent No. 7,161,351*, U.S. Patent and Trademark Office, Washington, DC, (2007).